machines

MDPI

Article

Performance Comparison of Two Architectures of 6R Articulated Robots

Giovanni Boschetti [1,*,†] and Teresa Sinico [2,†]

[1] Department of Industrial Engineering (DII), University of Padova, 35131 Padova, Italy
[2] Department of Management and Engineering (DTG), University of Padova, 36100 Vicenza, Italy
* Correspondence: giovanni.boschetti@unipd.it; Tel.: +39-049-827-6820
† The authors contributed equally to this work.

Abstract: This paper presents a comparison between two different 6R articulated robot architectures, one with a spherical wrist and the other with a non-spherical wrist and three consecutive parallel axes, which are found mainly in collaborative arms. The performance of the two architectures has been evaluated in terms of linear and rotational velocity using the Kinematic Directional Index (KDI). The results highlight the relation between the robot's velocity along a direction and the joint velocities. In this way, the proposed approach allows the evaluation of the best performance in a direction and the joints that limit the considered motion.

Keywords: directional index; serial robot; collaborative robot; performance evaluation; kinematics

Citation: Boschetti, G.; Sinico, T. Performance Comparison of Two Architectures of 6R Articulated Robots. *Machines* **2023**, *11*, 306. https://doi.org/10.3390/machines11020306

Academic Editor: Sever-Gabriel Racz

Received: 30 December 2022
Revised: 11 February 2023
Accepted: 16 February 2023
Published: 18 February 2023

1. Introduction

Since the advent of robots in industrial plants, 6 DOF articulated robots with a spherical wrist have been widely used for a variety of tasks. They are composed of six links connected by revolute joints and the spherical wrist consists of the last three joint axes that intersect at the same point. Therefore, the geometry structure of this type of robot satisfies the Pieper criterion [1]; i.e., three consecutive joint axes of the robot are parallel or intersect at a common point. Satisfying the Pieper criterion ensures that it is possible to find a certain amount of closed-form inverse kinematic solutions by the analytic method. This is particularly important for industrial robots, where real-time tasks require that the inverse kinematic solution is calculated within a certain known amount of time and that the robot configuration can be chosen arbitrarily.

Articulated robots with non-spherical wrists and that do not satisfy the Pieper criterion are also commonly used for particular industrial tasks, such as spray painting, where the wrist of the robot needs to be hollow [2,3]. For these robots, a numerical method needs to be used in order to solve the inverse kinematics, and therefore, the stability of the numerical solution and its convergence rate cannot be guaranteed. More recently, a new architecture found mainly in collaborative robots such as the Universal Robots UR-5 arm or TM5-700 has been proposed. This architecture is composed of six links connected by revolute joints, but the last three joints do not intersect at a common point; however, three consecutive joint axes (the second, third, and fourth) are parallels, and thus, the Pieper criterion is satisfied. The inverse kinematics of this structure, in particular for the Universal Robots UR-5/UR-10 arms, has been widely studied [4–7] as well as its singularities [8–10].

The difference between the articulated robot with a spherical wrist, which is currently the most widely used architecture for industrial robots, and the articulated robot with three consecutive joint axes, which is very common among the newest collaborative robots, is highlighted in Figure 1. In particular, the last three joint axes are depicted, and it can be seen that for the first architecture, they intersect at the same point (spherical wrist), and for the second one, they do not (non-spherical wrist). This work offers one of the first

investigations into the performance evaluation of these two different architectures in order to gain insights into their differences and similarities.

In general, a robot's performance depends on a variety of factors, such as the kinematics, the maximum speed, acceleration, and torque of the joint motors, and the control scheme. In this work, the performance of the two architectures will be conducted only in kinematic terms. To our knowledge, no one has so far studied how the kinematic differences of the two 6R robot architectures depicted in Figure 1 influence their performance. An effective way to compare different robot architectures is by using kinematic indexes [11,12]. In the literature, many kinematic indexes useful for the evaluation and comparison of robot manipulators have been proposed. Manipulability, the kinematic index introduced by Yoshikawa [13], is based on the Jacobian matrix of the velocity kinematic problem and allows the robot to be kept far from kinematic singularities, i.e., the robot configurations where the motion of the end-effector is restricted. Condition number, the index introduced by Salisbury [14], offers a comprehensive analysis of the workspace isotropy, i.e., the ratio between the maximum and minimum performance of the robot. Minimum singular value, kinematic isotropy [15], conditioning indexes [16], and dexterity analyses [17] are also based on the Jacobian matrix and provide a variety of information about a robot's performance throughout its workspace. However, the use of these approaches raised some problems [18] that have been resolved as these methods have evolved; a modern performance index must provide information in a summarized form, such as a value, on the behavior of the manipulator in its workspace. The key characteristics of a modern performance index are its independence from the unit of measurement [19–24] and also its independence from the reference system [25,26]. Recentely, two interesting optimization frameworks have been developed for the workspace analysis and visualization so to improve the design of industrial robots [27,28]. Nevertheless, most of the kinematic indexes found in the literature provide information about the behavior of the robot at a specific point in the workspace, not considering the direction of motion.

Taking into account these limitations, the Kinematic Directional Index (KDI) [29] was proposed, and its effectiveness has been proved. This index aims to determine the region in which a serial robot reaches its maximum translational velocity. Given the direction of the main robot movements, the KDI index is particularly effective in identifying the best location in the robot's workspace for that task and, therefore, drastically reducing the time taken to complete it. In this research, because we were interested in finding the area of maximum velocity with respect to a direction of interest, the KDI index was used to compare the 6R articulated robot with a spherical wrist and the 6R articulated robot with a non-spherical wrist. Since the main difference between the two robot architectures lies in their wrist, which plays a crucial role in terms of angular velocity, the KDI index was also exploited to evaluate the robot performance in terms of maximum rotational velocity.

The paper is organized as follows: in Section 2, the KDI performance index is defined and formulated. Section 3 provides some preliminary considerations on the kinematic parameters of the two robot architectures and on the maximum speed of each joint. This is followed by Sections 4 and 5, which provide a comparison of the performance of the two 6R articulated robots in terms of linear and angular velocity. Finally, in Section 6, the conclusions are addressed.

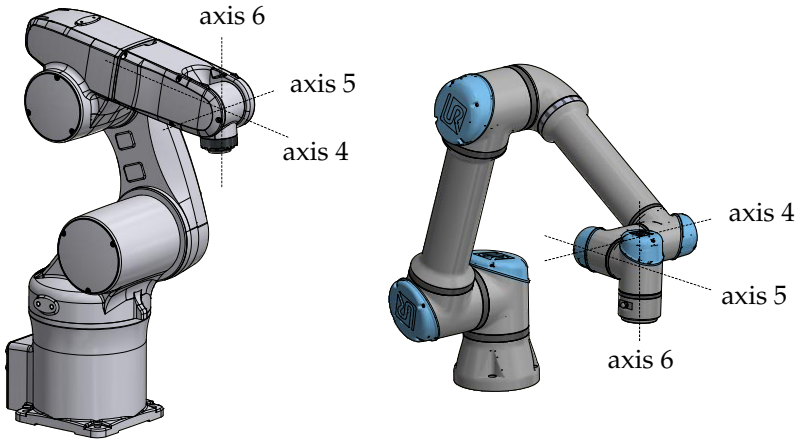

Figure 1. Different robot architectures: (**left**) articulated robot with a spherical wrist (Adept Viper S650), (**right**) articulated robot with non-spherical wrist and three consecutive parallel joint axes (Universal Robots UR5).

2. The KDI Performance Index

The KDI performance index was first proposed and validated in [29]. This kinematic index allows the evaluation of the behavior of a serial manipulator in its workspace in terms of linear velocity among a certain direction. This index, like many other kinematic indexes, is based on the analysis of the Jacobian matrix $\boldsymbol{J}$. The forward velocity kinematic equation is defined by Equation (1):

$$\dot{\boldsymbol{x}} = \boldsymbol{J}\dot{\boldsymbol{q}}, \tag{1}$$

where $\dot{\boldsymbol{x}}$ is the velocity vector in the Cartesian space and $\dot{\boldsymbol{q}}$ is the velocity vector in the joint space. Once the direction of interest is defined, the velocities along the axes that are normal to the direction of interest are set as null values as well as the angular velocities. If one considers the direction of interest along the x axis, the velocity in this direction for a non-redundant robot with n degrees of freedom can be defined as follows in (2).

$$\begin{Bmatrix} \dot{x} \\ \vdots \\ 0 \end{Bmatrix} = \begin{bmatrix} j_{1,1} & \cdots & j_{1,n} \\ \vdots & \ddots & \vdots \\ j_{n,1} & \cdots & j_{n,n} \end{bmatrix} \begin{Bmatrix} \dot{q}_1 \\ \vdots \\ \dot{q}_n \end{Bmatrix} \tag{2}$$

When the direction of interest d is not along the x axis, a rotation matrix $\boldsymbol{R}$ must be defined: this matrix aligns the x axis to the direction of interest d. Let us define $\boldsymbol{J_R}$ as the Jacobian matrix rotated by the matrix $\boldsymbol{R}$, which can be found using Equation (3):

$$\boldsymbol{J_R} = \begin{bmatrix} \boldsymbol{R} & 0 \\ 0 & \boldsymbol{R} \end{bmatrix} \boldsymbol{J} = \begin{bmatrix} j_{R\,1,1} & \cdots & j_{R\,1,n} \\ \vdots & \ddots & \vdots \\ j_{R\,n,1} & \cdots & j_{R\,n,n} \end{bmatrix}. \tag{3}$$

Therefore, the velocity in the d direction can be calculated using Equation (4).

$$\begin{Bmatrix} \dot{d} \\ \vdots \\ 0 \end{Bmatrix} = \begin{bmatrix} j_{R\,1,1} & \cdots & j_{R\,1,n} \\ \vdots & \ddots & \vdots \\ j_{R\,n,1} & \cdots & j_{R\,n,n} \end{bmatrix} \begin{Bmatrix} \dot{q}_1 \\ \vdots \\ \dot{q}_n \end{Bmatrix} \tag{4}$$

The value of KDI is identified by the letter K and is defined as the maximum value assumed by $\dot{d}$ as highlighted in Equation (5).

$$K = \max(\dot{d}) \tag{5}$$

For a non-redundant robot, when a robot moves at its maximum speed in the direction of interest d, at least one joint motor is working at its maximum speed. Therefore, to find the solution to this problem, the velocity in the direction of interest $\dot{d}$ can be set to a fictitious value of 1, and the fictitious motor velocities can be easily calculated, since the following problem is defined by a linear system (6) where the number of unknowns is equal to the number of equations.

$$\begin{Bmatrix} 1 \\ \vdots \\ 0 \end{Bmatrix} = \boldsymbol{J_R} \begin{Bmatrix} \dot{q}_1 \\ \vdots \\ \dot{q}_n \end{Bmatrix} \tag{6}$$

Once the linear problem in Equation (6) is solved, all the values of $\dot{q}_i$ are known. The motor that limits the robot's performance is the one that has the velocity nearest to its maximum value. To easily find this motor (p) and its ratio with respect to its maximum velocity, let us define the maximum value achieved by the ratios between each joint speed and its maximum as follows by Equation (7):

$$\frac{1}{K} = \frac{\dot{q}_p}{\dot{q}_{p,\max}} = \max\left(\frac{\dot{q}_1}{\dot{q}_{1,\max}}, \ldots, \frac{\dot{q}_n}{\dot{q}_{n,\max}}\right) \tag{7}$$

$1/K$ is the maximum ratio between a joint speed and its maximum velocity, and this value is given by the joint p whose speed is closest to its maximum. This value can also be greater than 1, which happens because the solution to the problem is proposed using fictitious velocities. K identifies the KDI and also the maximum speed that the robot can reach in the chosen direction of interest d.

2.1. KDI Performance Index for the Investigated Architectures

As mentioned, the KDI index is based on the analysis of the Jacobian matrix $\boldsymbol{J}$. It should be noted that both architectures depicted in Figure 1 present six revolute joints. If the Denavit Hartenberg convention is used to attach the reference frames to the links of the manipulators, their Jacobian matrix can be computed by Equation (8):

$$\boldsymbol{J} = \begin{bmatrix} \boldsymbol{j_{p_1}} & \boldsymbol{j_{p_2}} & \boldsymbol{j_{p_3}} & \boldsymbol{j_{p_4}} & \boldsymbol{j_{p_5}} & \boldsymbol{j_{p_6}} \\ \boldsymbol{j_{\omega_1}} & \boldsymbol{j_{\omega_2}} & \boldsymbol{j_{\omega_3}} & \boldsymbol{j_{\omega_4}} & \boldsymbol{j_{\omega_5}} & \boldsymbol{j_{\omega_6}} \end{bmatrix}, \tag{8}$$

where $\boldsymbol{j_{p_i}} = \boldsymbol{z_i} \times (\boldsymbol{O_{EE}} - \boldsymbol{O_i})$ and $\boldsymbol{j_{\omega_i}} = \boldsymbol{z_i}$. For an articulated robot with a spherical wrist, the velocity of the last three joints does not affect the linear velocity of the center of the spherical wrist: for this reason, $\boldsymbol{j_{p4}}$, $\boldsymbol{j_{p5}}$, and $\boldsymbol{j_{p6}}$ are null terms. Consequently, in the previous work, in the computation of the KDI for this type of robot, only the first 3×3 submatrix was considered. However, for an articulated robot with three consecutive parallel axes, such as the Universal Robots UR-5 arm, all six joints contribute to both the translational and rotional motion of the end-effector. Therefore, to compute the KDI index, it is necessary to take into account the full Jacobian matrix. In this research, the full Jacobian matrix was used to calculate the KDI index for both the articulated robot with a spherical wrist and the typical collaborative robot with three consecutive parallel joint axes.

2.2. KDI Exploited for the Rotational Velocity

In the previous study, the performance of the robot was not explored in terms of angular velocity. In this research, because we were interested in evaluating the performance of the two 6R articulated robots, which differ mainly in the structure of the wrist, the KDI was also used to evaluate the two architectures in terms of rotational velocity. Equation (1) can be rewritten as follows in Equation (9):

$$\begin{Bmatrix} \dot{x} \\ \dot{y} \\ \dot{z} \\ \omega_x \\ \omega_y \\ \omega_z \end{Bmatrix} = \boldsymbol{J} \begin{Bmatrix} \dot{q}_1 \\ \dot{q}_2 \\ \dot{q}_3 \\ \dot{q}_4 \\ \dot{q}_5 \\ \dot{q}_6 \end{Bmatrix}. \tag{9}$$

For example, to evaluate robot performance in terms of angular velocity ω_x, the rotational velocity ω_x is set to a fictitious value of 1 and linear velocities as well as ω_y and ω_z are set as null values. Motor velocities can then be found by resolving the linear system above, and the KDI can be computed using Equation (7). To evaluate angular velocities around different axes, a Jacobian rotated matrix $\boldsymbol{J_R}$ can also be defined. However, it is worth mentioning that to solve the linear system (9), the Jacobian matrix $\boldsymbol{J}$ must be nonsingular ($\det(\boldsymbol{J}) \neq 0$). When $\det(\boldsymbol{J}) = 0$, the robot is in a singular configuration and loses one or more degrees of freedom. When the robot approaches a singular configuration, the KDI value approaches as zero; therefore, when $\det(\boldsymbol{J}) = 0$ and the linear system (9) cannot be solved, the KDI is set as a null value.

3. Preliminary Considerations

3.1. Kinematic Parameters of the Two 6R Articulated Robots

To properly and objectively compare the performance of the two 6R articulated robots, the one with a spherical wrist and the one with a non-spherical wrist and three consecutive parallel joint axes, they need to have the same workspace. The workspace depends on the lengths of the links of the manipulator: these lengths have been chosen with the aim of obtaining a workspace with the external radius of $r_{ext} = 900\,\text{mm}$. For the articulated robot with a spherical wrist, the kinematic parameters are listed in Table 1, which are expressed as Denavit Hartenmberg parameters. For an articulated robot with a spherical wrist, the dimensions of the workspace depend mainly on a_2 and d_4; the lengths of the considered links are $a_1 = 120\,\text{mm}$, $a_2 = 385\,\text{mm}$, $a_3 = 110\,\text{mm}$ and $d_4 = 385\,\text{mm}$. For the linear velocity analysis carried out in Section 4, the last reference frame was considered to be in the center of the spherical wrist, so d_6 was set as a null value. Instead, for the angular velocity analysis carried out in Section 5, the last reference frame was considered to be on the robot flange and d_6 was set as $d_6 = 100\,\text{mm}$. It is also worth noting that for the articulated robot with a spherical wrist, the range of the first joint was assumed to be $\pm 180°$, although for this type of robot, it is also common for that range to be $\pm 170°$.

Table 1. Denavit Hartenberg table of the articulated robot with a spherical wrist.

i	$T_{i,i-1}$	α_{i-1}	a_{i-1}	θ_i	d_i
1	$T_{1,0}$	0	0	θ_1	0
2	$T_{2,1}$	$-\pi/2$	a_1	θ_2	0
3	$T_{3,2}$	0	a_2	θ_3	0
4	$T_{4,3}$	$-\pi/2$	a_3	θ_4	d_4
5	$T_{5,4}$	$\pi/2$	0	θ_5	0
6	$T_{6,5}$	$-\pi/2$	0	θ_6	d_6

On the other hand, in Table 2, the complete Denavit Hartenberg table of the considered articulated robot with a non-spherical wrist is defined. For this robot, the dimensions of the workspace depend mainly on a_2 and a_3. The lengths of the links, which are used for the computation of the Jacobian matrix, are $d_1 = 150\,\text{mm}$, $a_2 = 400\,\text{mm}$, $a_3 = 400\,\text{mm}$, $d_4 = 150\,\text{mm}$, $d_5 = 100\,\text{mm}$ and $d_6 = 100\,\text{mm}$.

Table 2. Denavit Hartenberg table of the articulated robot with a non-spherical wrist and three consecutive parallel joint axes.

i	$T_{i,i-1}$	α_{i-1}	a_{i-1}	θ_i	d_i
1	$T_{1,0}$	0	0	θ_1	d_1
2	$T_{2,1}$	$\pi/2$	0	θ_2	0
3	$T_{3,2}$	0	a_2	θ_3	0
4	$T_{4,3}$	0	a_3	θ_4	d_4
5	$T_{5,4}$	$\pi/2$	0	θ_5	d_5
6	$T_{6,5}$	$-\pi/2$	0	θ_6	d_6

3.2. Maximum Joint Velocities

From Equation (7), it can be observed that the value of the KDI index depends not only on the value of the maximum joint velocities of the robot but also on their relative values from each other. For this reason, the maximum speed joint velocities of popular industrial robots with both architectures have been investigated. Table 3 provides an overview of the maximum joint velocities of popular articulated industrial robots with a spherical wrist: it shows a clear trend of increasing the maximum speed of the last three joints. In particular, the last motor joint usually has a maximum speed that is twice the maximum speed of the first motor.

Table 3. Maximum joint velocities of popular articulated robots with a spherical wrist.

	J1 (°/s)	J2 (°/s)	J3 (°/s)	J4 (°/s)	J5 (°/s)	J6 (°/s)
Adept Viper S650	328	300	375	375	375	600
ABB IRB 1300	280	228	330	500	415	720
ABB IRB 6790	100	90	90	170	120	190
FANUC LR Mate 200ic	350	350	400	450	450	720
Yaskawa Motoman MH50	180	178	178	250	250	360
FANUC R-2000ib/165F	110	110	110	150	150	220
ABB IRB 4600-45/2.05	175	175	175	250	250	360

In Table 4, the maximum joint velocities of popular collaborative robots with a non-spherical wrist and three consecutive parallel joint axes are reported. It can be noted that robot manufacturers assign maximum joint speeds in different ways: some of these robots present a higher maximum speed for the last three joints, whereas some others have the same maximum speed for each of the joint motors. In this work, the correct ratio between these velocities was investigated for both architectures.

Table 4. Maximum joint velocities of popular collaborative robots with a non-spherical wrist and three consecutive parallel joint axes.

	J1 (°/s)	J2 (°/s)	J3 (°/s)	J4 (°/s)	J5 (°/s)	J6 (°/s)
Omron TM5-700	180	180	180	225	225	225
Dobot Nova Series	135	135	135	135	135	135
Universal Robots UR-5	180	180	180	180	180	180
Elephant Robotics MyCobot	225	225	225	225	225	225
Hanwha Corporation HCR-3A	180	180	180	360	360	360
Rainbow Robotics RB5-850	180	180	180	180	180	180

4. KDI Analysis for the Linear Velocity

4.1. Point Sets

Given the proper Jacobian matrix, it is possible to calculate the KDI at any point in the workspace and in any direction of interest d. Given a task to perform along a certain

direction d, this is useful for identifying areas where the robot reaches its maximum speed with respect to that direction. The world and the end-effector reference frames of the two robot architectures are depicted in Figure 2. In particular, the world reference frame of the articulated robot with a spherical wrist is assumed to be at the intersection between the first and second joint axes. Conversely, the world reference of the articulated robot with a non-spherical wrist is assumed to be at the bottom of the manipulator, with z_0 coincident with the axis of the first joint. The performance of the two different architectures has been evaluated in the horizontal plane with the highest reach distance, which is the plane where the center of the wrist is at the same height as the shoulder. The set of points considered was given, for both architectures, by ten points along any radial direction with an angular step of ten degrees. In Figure 3, the two sets of points are depicted together with the limits of the workspace. It can be seen that although the external radius r_{ext} of the workspace is the same for the two architectures, the internal radius is greater in the articulated robot with a spherical wrist.

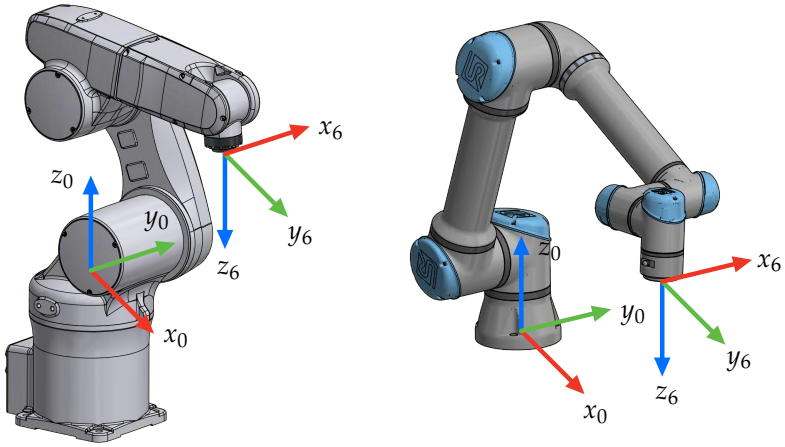

Figure 2. Position of the world and end-effector reference frames (**left**) articulated robot with a spherical wrist and (**right**) articulated robot with non-spherical.

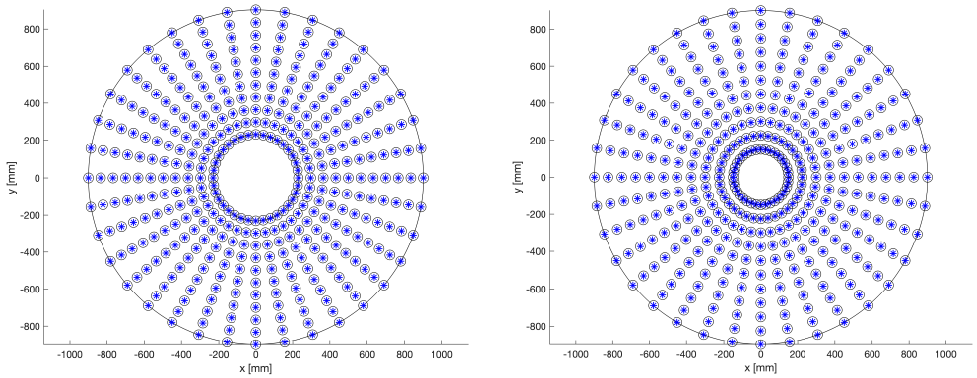

Figure 3. Point sets in which the experimental analysis was performed for the articulated robot with a spherical wrist (**left**) and for the articulated robot with a non-spherical wrist and three consecutive joint axes (**right**).

4.2. KDI along the Direction of the X Axis

Most robot applications consist of picking and placing objects, moving first among the z axis to pick the part, then horizontally among a certain plane, and then again along the z axis to place the part. For this reason, the direction of interest was first set along the x axis. For each set of coordinates (x, y, z), the orientation was set to $(\alpha = 0°, \beta = 180°, \gamma = 180°)$ expressed as Euler angles (z, y', z'' rotation sequence), and the inverse kinematic problem was solved. With the set of joint values obtained, the Jacobian matrix was calculated. By

inverting the Jacobian matrix, it was then possible to compute the joint velocities, consider their absolute value, and divide it by their relative maximum joint velocity. For a given point, the maximum value of the division $q_i/q_{i,\max}$ was taken as $1/K$, and then K is the KDI value for that specific point. As mentioned above, the value of the KDI index depends on $\dot{q}_{i,\max}$: the maximum joint speed was first set as 100 °/s for each joint. Figure 4 shows the trend of the KDI value obtained in the workspace for both architectures. The whole horizontal plane of the workspace is depicted in a color that represents the value of the obtained KDI from blue (lowest values) to yellow (highest values). The region of the workspace depicted in blue denotes an area of the workspace where the KDI assumes a low value and therefore an area of the workspace where the robot cannot reach a high speed when performing a movement along the x axis. In contrast, the region of the workspace depicted in yellow denotes an area where the KDI assumes a high value and the robot can reach a high speed when moving along the direction of the x axis. Figure 4 shows no considerable difference between the two architectures, except that the graph for the articulated robot with a non-spherical wrist is not symmetrical and the KDI assumes low values not only near the outer limit of the workspace but also near its inner limit.

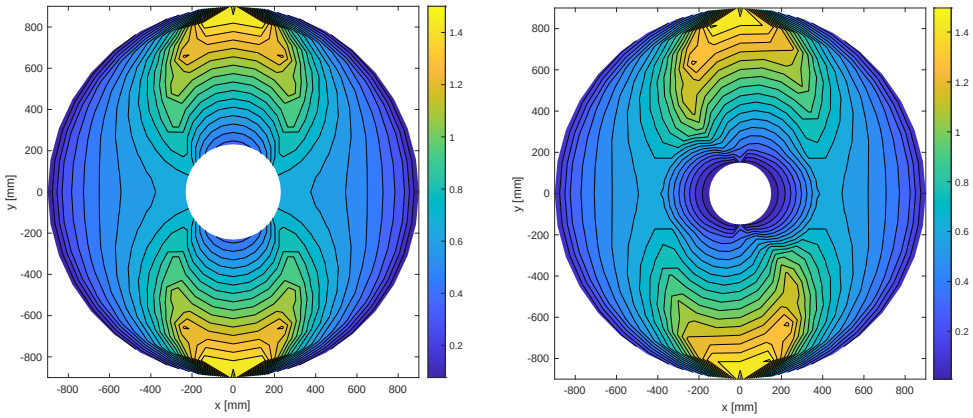

Figure 4. KDI investigation in the workspace along the direction of the x axis with maximum joint speed set as 100 °/s for each joint for the articulated robot with a spherical wrist (**left**) and for the articulated robot with a non-spherical wrist and three consecutive joint axes (**right**).

The maximum value of the KDI for the articulated robot with a spherical wrist is $KDI_{\max} = 1.5715$, while the maximum value of the KDI for the articulated robot with a non-spherical wrist is $KDI_{\max} = 1.5708$. Overall, these results indicate that the maximum KDI value is the same for the two architectures, but the trend of the KDI is slightly different. For both architectures, there is only a relatively small region in the workspace where the robot can reach a high speed along the direction of the x axis. By observing Equation (7), it is clear that the KDI depends linearly on the maximum velocity of the joint axes: if the maximum velocity of each joint is set as 200 °/s, the KDI graphics in the workspace remain the same as the one depicted in Figure 4, but the maximum value of the KDI doubles, and so on. For every other direction in the same plane, obtained with a rotational matrix $\boldsymbol{R}$ along the z axis, the trend in the workspace remains the same, which is rotated by the chosen angle. If the maximum joint speed is the same for each joint, Figure 4 shows no substantial differences between the two architectures: they both reach their maximum linear velocity in the same area of the workspace.

4.2.1. Motor Nearest to Its Maximum Velocity

It is particularly interesting to analyze, for the different points in the workspace, which is the motor p, i.e., the motor that is closest to its maximum velocity and therefore the bottleneck. Understanding which motor is the p motor will greatly contribute to the optimal choice of the maximum values of each joint speed to maximize the area of the workspace in which a high value of linear velocity can be obtained along a certain direction. Figure 5

shows, for each point considered for both architectures, the motor p nearest to its maximum velocity: each point is depicted in a color that represents the motor working closest to its maximum speed.

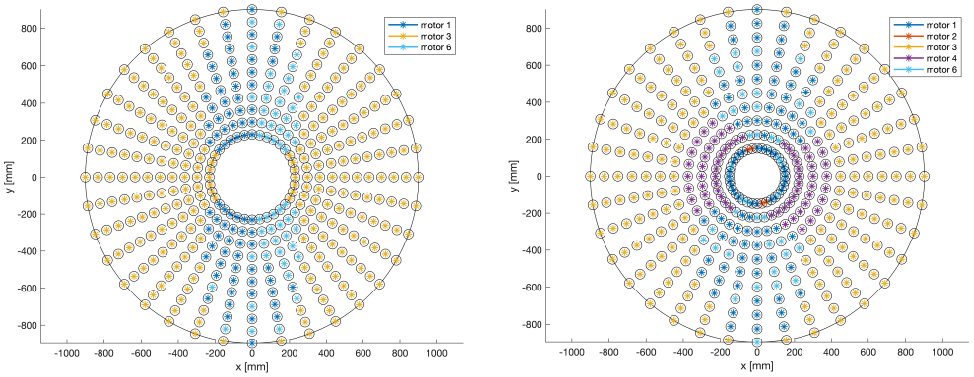

Figure 5. Motor p nearest to its maximum velocity when the direction of interest is along the x axis and the maximum joint speed is set as 100 °/s for each joint for the articulated robot with a spherical wrist (**left**) and for the articulated robot with a non-spherical wrist and three consecutive joint axes (**right**).

For the articulated robot with a spherical wrist, Figure 5 shows a strong correlation between robot performance in terms of linear velocity in a horizontal plane and the maximum speed of the third joint, which represents the motor p in the majority of the workspace. From Figure 5, it can also be observed that there is a region of the workspace where the motor that limits the robot's performance is either motor 1 or motor 3. In this region, for the chosen orientation, $(\alpha = 0°, \beta = 180°, \gamma = 180°)$ expressed as Euler angles, $\dot{q}_1$ and $\dot{q}_3$ always assume the same value. For this reason, if their maximum speed is the same, both motors represent motor p: the fact that in this region, in Figure 5, only one or the other is depicted depends on the approximation done by MATLAB. However, it should be noted that the region where the motor p is the motor of the first or third joint is a region where the KDI already assumes a high value. For the articulated robot with a non-spherical wrist, Figure 5 reveals that there is still a wide region of the workspace where the motor working nearest its maximum velocity is the third joint motor, but there is also a significantly wide region near the inner limit of the workspace where the motor p is the fourth joint motor. Similarly to the articulated robot with a spherical wrist, there is a region near $x = 0$ where the KDI already assumes a high value and the motor p is motor 1 or 6; in this case, $\dot{q}_1$ and $\dot{q}_3$ do not assume the same value. Interestingly, these results show that for an articulated robot with a non-spherical wrist and three consecutive parallel axes, even though the motor of the third joint plays a crucial role in the robot performance in terms of linear velocity in a horizontal plane, the motors of the first, fourth, and fifth joint also contribute to the robot's linear speed. These results indicate that in order to obtain a high value of the KDI in a wider portion of the workspace, for the articulated robot with a spherical wrist, the maximum speed of the third joint should be increased, whereas for the articulated robot with a non-spherical wrist, the maximum speed of both the third and fourth joint should be increased to enhance the robot performance.

4.2.2. KDI along the Direction of the X Axis on Different Planes

To extend the obtained results, the KDI value could also be calculated on different planes. For example, Figure 6 shows the trend of the KDI value obtained in four different planes of the workspace for both architectures. It can be noted that the highest values of KDI are reached, for both architectures, in the lower plane (which is the plane with the highest reach distance considered before). Moreover, the KDI trend for the two architectures is slightly different, but the main difference that can be observed from Figure 6 is that for

the articulated robot with a non-spherical wrist, there is always a region of the workspace (near $x = 0$ and $y = 0$) that cannot be reached, while for the articulated robot, there is not.

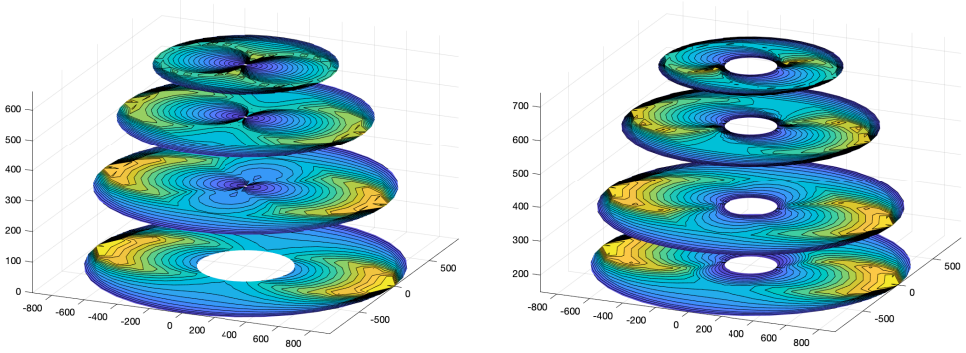

Figure 6. KDI investigation in the workspace on different planes for the articulated robot with a spherical wrist (**left**) and for the articulated robot with a non-spherical wrist and three consecutive joint axes (**right**).

4.2.3. KDI along the Direction of the X Axis with Modified Maximum Joint Speeds

According to the results presented in Section 4.2.1, the KDI value for the given sets of points along the direction of the x axis was then calculated with modified values of the maximum joint speed: in particular, the maximum speed of the third joint was set as 200 °/s, while the other maximum joint speeds were left as 100 °/s. The trend of the KDI obtained for the two architectures is depicted in Figure 7.

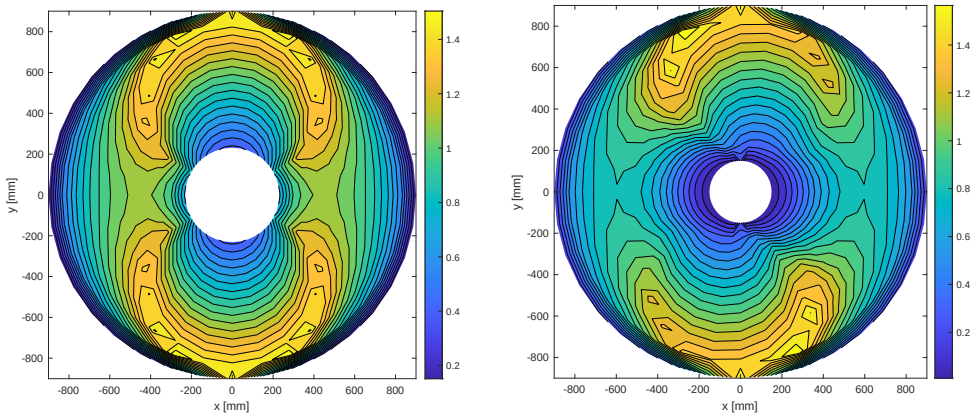

Figure 7. KDI investigation in the workspace along the direction of the x axis with maximum joint speed set as 200 °/s for the third joint and as 100 °/s for the other joints for the articulated robot with a spherical wrist (**left**) and for the articulated robot with a non-spherical wrist and three consecutive joint axes (**right**).

Although the maximum value of the KDI remains approximately the same ($KDI_{\max} = 1.5715$ for the articulated robot with a spherical wrist and $KDI_{\max} = 1.6429$ for the articulated robot with three consecutive axes), Figure 7 shows a considerable difference from Figure 4 in terms of the trend of the KDI index. For both manipulators, there is a much wider region of the workspace with a high value of the KDI, which confirms the strong correlation between the linear velocity of the robot and the maximum speed of the third joint, although this correlation is stronger for the articulated robot with a spherical wrist. The KDI value for the given sets of points was also calculated with the maximum speed of the third and fourth maximum joint speed set as 200 °/s and the remaining joint maximum speed left as 100 °/s. The trend of the KDI obtained with this set of maximum joint speeds is shown in Figure 8.

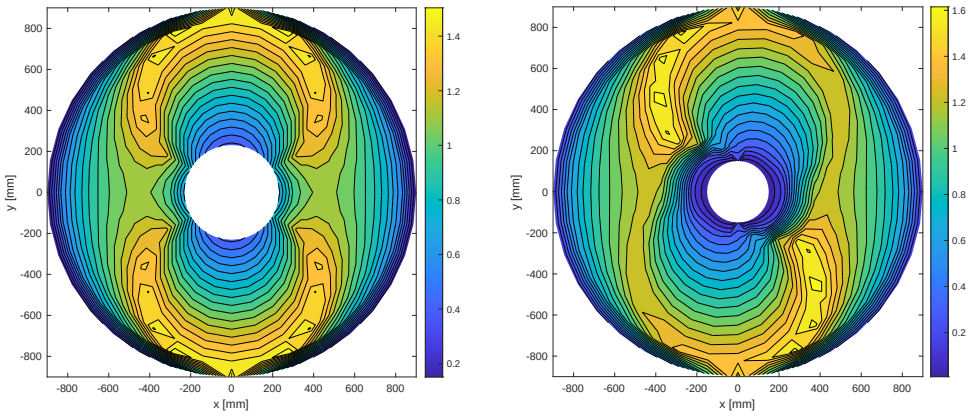

Figure 8. KDI investigation in the workspace along the direction of the x axis with maximum joint speed set as 200 °/s for the third and fourth joint and as 100 °/s for the remaining joints for the articulated robot with a spherical wrist (**left**) and for the articulated robot with a non-spherical wrist and three consecutive joint axes (**right**).

The trend of the KDI index obtained verifies that for an articulated robot with a spherical wrist, the maximum speed of the fourth joint does not affect the linear velocity in a horizontal plane, for Figures 7 and 8 are exactly the same. On the contrary, for the articulated robot with a non-spherical wrist, Figure 8 reveals a relationship between the KDI trend in the workspace and the maximum speed of the fourth joint: compared to Figure 7, Figure 8 presents a much wider area of the workspace characterized by a high value of the KDI index, which is consistent with the observations provided in Section 4.2.1. These findings indicate that for maximizing the area of the workspace where the robot reaches a high value of speed along the direction of the x axis for a robot with a spherical wrist, it is necessary to increase the value of the maximum speed of the third joint, while for a robot with a non-spherical wrist, it is necessary to increase the value of the maximum speed of both the third and fourth joint.

4.3. KDI along the Direction of the Z Axis

The direction of interest was then set along the z axis, the orientation was left as $(\alpha = 0°, \beta = 180°, \gamma = 180°)$ expressed as Euler angles, and the maximum joint speed was restored as 100 °/s for each joint. The investigation was carried out in the horizontal plane with the highest reach for both architectures. The trend of the KDI index, for the two 6R articulated robots, is shown in Figure 9: the trend is similar for the two architectures, but the articulated robot with a non-spherical wrist has a wider area of the workspace, near its inner and outer limit, where the KDI index assumes a low value.

The maximum value of the KDI along the direction of the z axis for the articulated robot with a spherical wrist is $KDI_{\max} = 1.3621$, while the maximum value of the index for the articulated robot with three consecutive axes is $KDI_{\max} = 0.9839$. These numbers suggest that given the same outside radius of the workspace and the same maximum speed for each joint, the articulated robot with a spherical wrist performs better in terms of linear velocity along the z axis. It is important to underline that when the best performance is achieved in regions close to the maximum reachable distance, the motion should be properly planned to avoid the robot reaching the limit of the workspace

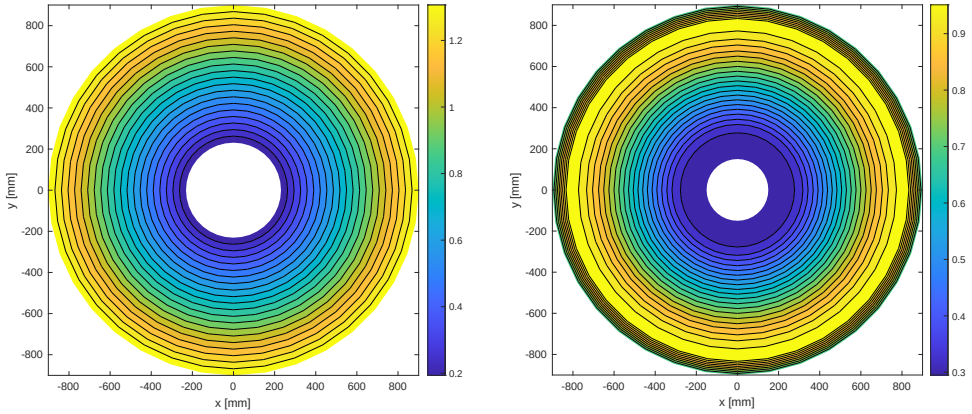

Figure 9. KDI investigation in the workspace along the direction of the z axis with maximum joint speed set as 100 °/s for each joint for the articulated robot with a spherical wrist (**left**) and for the articulated robot with a non-spherical wrist and three consecutive joint axes (**right**).

Motor Nearest to Its Maximum Velocity

To contribute to our understanding of the influence of each joint maximum speed on robot performance, it is interesting to analyse, for the different points in the workspace, which is the motor p that limits the robot's linear velocity along the direction of the z axis. In Figure 10, the set of points for both architectures is depicted in a color that represents, for each point, the motor p.

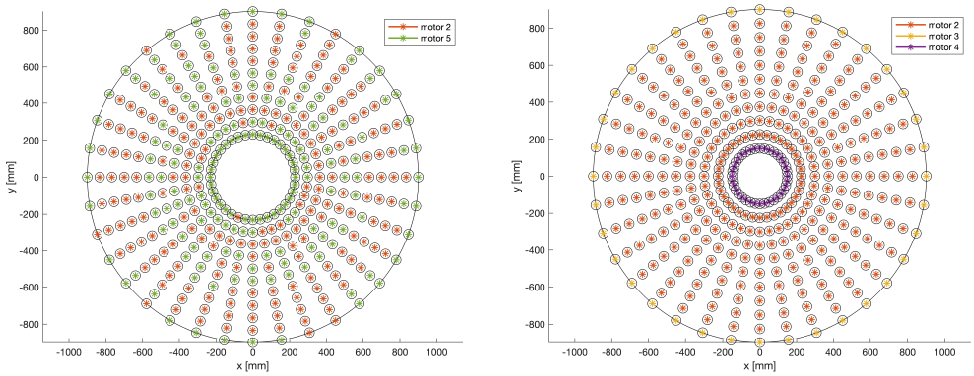

Figure 10. Motor p nearest to its maximum velocity when the direction of interest is along the z axis and the maximum joint speed is set as 100 °/s for each joint for the articulated robot with a spherical wrist (**left**) and for the articulated robot with three consecutive joint axes (**right**).

For the articulated robot with a spherical wrist, Figure 10 shows that the performance of the robot in terms of linear velocity along the z axis depends on the maximum joint speed of the second and fifth joints. For the chosen orientation, at all points considered in the workspace, $\dot{q}_2$ and $\dot{q}_5$ always assume the same value. As a result, both motors represent the motor p, and in the figure, it is depicted as one or the other according to the approximation done by MATLAB. On the other hand, for the articulated robot with a non-spherical wrist, Figure 10 reveals that in the vast majority of the workspace, except at its limits, the motor p is motor 2. This has a significant implication in terms of robot design when aiming to maximize the linear velocity along the z direction while maintaining the same orientation: for the articulated robot with a non-spherical wrist it is sufficient to increase the maximum speed of the second joint, while for the articulated robot with a spherical wrist, it is necessary to increase both the maximum speed of the second and of the fifth joint.

5. KDI Analysis for the Angular Velocity

Firstly, it is worth mentioning that when evaluating the linear velocity, it is interesting to plot the KDI index in the workspace while maintaining the same orientation (α, β, γ) for the end-effector in order to understand which is the best area of the workspace to perform a movement along a certain direction. On the other hand, when evaluating the angular velocity, the orientation changes, and it is not significant to plot the KDI trend in the workspace. It is more significant to select a specific point in the workspace and, at that point, evaluate the KDI while changing the orientation of the end-effector.

5.1. KDI for the Angular Velocity ω_x

As mentioned above, it is also interesting to compare the two robot architectures in terms of angular velocity ω_x, ω_y, and ω_z. Clearly, for the orientation $(\alpha = 0°, \beta = 180°, \gamma = 180°)$ expressed as Euler angles, the angular velocity ω_z of both manipulators is strongly correlated with the maximum velocity of the sixth joint. Instead, in the first place, it is more significant to calculate the KDI for the angular velocity ω_x. The analysis of the KDI in terms of angular velocity was carried out as follows: first, a specific set of points was chosen. The analysis was carried out in the highest reach plane, y was set as $y = 0$ and x was set to vary from $x = 280$ mm to 650 mm with a step of 50 mm. For each point, to evaluate the rotational velocity ω_x, the orientation was varied from $(\alpha = -90°, \beta = 0°, \gamma = 90°)$ to $(\alpha = -90°, \beta = 360°, \gamma = 90°)$ expressed as Euler angles, with an angular step of 10° in terms of β. For each point and each orientation, the KDI was calculated for both architectures, and the results obtained are shown in Figure 11.

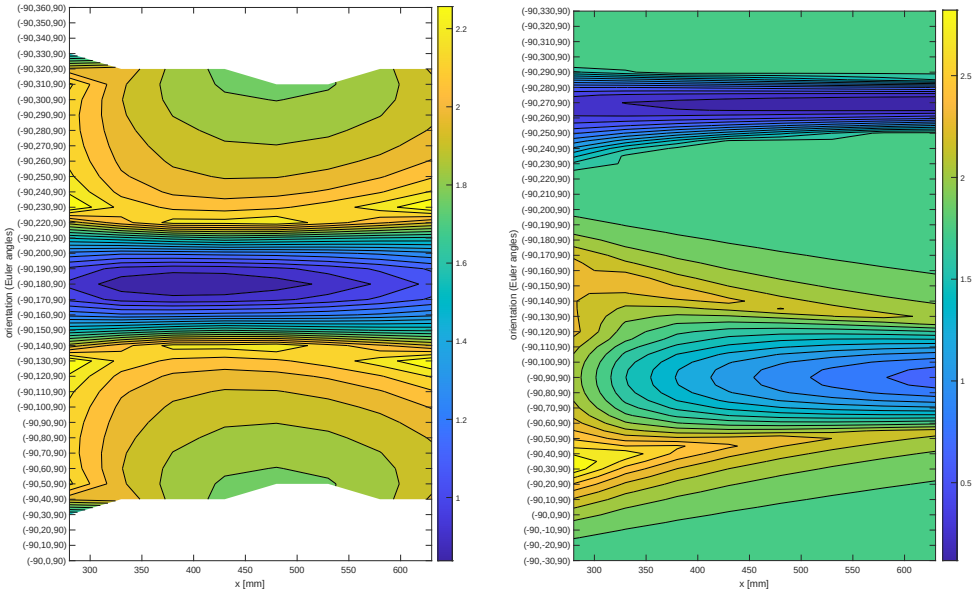

Figure 11. KDI investigation in terms of angular velocity ω_x with maximum joint speed set as 100 °/s for each joint for the articulated robot with a spherical wrist (**left**) and for the articulated robot with a non-spherical wrist and three consecutive joint axes (**right**).

From Figure 11, the first thing that can be observed is that for the articulated robot with a spherical wrist, not all orientations can actually be reached. This is due to the limited range of the fifth joint, which is typically between $\theta_5 = \pm 120°$ and $\theta_5 = \pm 140°$ depending on the different manufacturers. For this analysis, the range of the fifth joint was considered to be $\theta_5 = \pm 140°$. On the other hand, for an articulated robot with a non-spherical wrist and three parallel consecutive axes, the range of the fifth joint is typically $\theta_5 = \pm 360°$, and therefore, all orientations considered can be reached by the robot. For the articulated robot with a spherical wrist, among the points considered, the lowest value of the KDI ($KDI_{\text{min}} = 0.83$) was reached at $x = 400$ mm and $(\alpha = -90°, \beta = 180°, \gamma = 90°)$: this

configuration is shown at the left of Figure 12 and corresponds to a configuration near the wrist singularity, where the fourth and sixth axes are close to being coincident and θ_5 is close to a null value. Around this configuration, the KDI index assumes values that vary from 2.2 to 1.8. For the articulated robot with a non-spherical wrist and three consecutive parallel axes, the lowest value of the KDI ($KDI_{\text{min}} = 0.15$) was assumed for $x = 450\,\text{mm}$ and the orientation was $(\alpha = -90°, \beta = 0°, \gamma = 90°)$. The robot configuration in this condition is shown at the right of Figure 12: the fourth and sixth joint axes are almost aligned, and the robot is close to the wrist alignment singularity ($\theta_5 = 0°$ or $\theta_5 = \pm 180°$), which is one of the three types of singularity that can be found in this type of robot [8–10]. For this robot, the other orientation around which the KDI assumes low values is $(\alpha = -90°, \beta = 0°, \gamma = 90°)$: this configuration is similar to the one depicted at the right of Figure 12, as the fourth and sixth joint axes are almost aligned. Between the two configurations characterized by the lowest values of the KDI index, the KDI assumes an almost uniform value of 1.8.

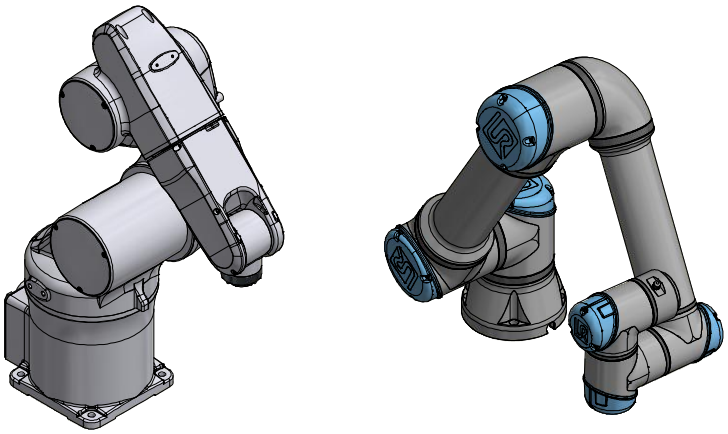

Figure 12. Configurations in which the two 6R architectures assume their lowest value of the KDI index in terms of angular velocity ω_x: (**left**) articulated robot with a spherical wrist, (**right**) articulated robot with a non-spherical wrist.

These findings show that the difference in wrist structure determines, in fact, a difference in terms of angular velocity performance, which is lower but more uniform for the typical collaborative arm. These results also indicate that the KDI successfully identifies the singularities. In addition, it should be noted that overall, the non-spherical wrist of the articulated robot with three consecutive parallel axes such as the Universal Robots UR-5 is more versatile, because each joint has a range of $\pm 360°$, while the articulated robot has a limited range of joint 5.

5.2. KDI for the Angular Velocity ω_y

The same analysis was also performed in terms of angular velocity ω_y: the same set of points considered for the angular velocity ω_x was used, but in this case, the orientation was varied from $(\alpha = 0°, \beta = 0°, \gamma = 180°)$ to $(\alpha = 0°, \beta = 360°, \gamma = 180°)$ with an angular set of 10° in terms of β. For each point and each orientation, the KDI was calculated for both architectures, and the results obtained are shown in Figure 13.

Similarly to the analysis conducted for the angular velocity ω_x, the first thing that emerges from Figure 13 is that for the articulated robot with a spherical wrist, not all orientations can be reached due to the limited range of the fifth joint. However, Figure 13 shows that the trend of the KDI index for the rotational velocity ω_y is similar for the two architectures. For the articulated robot with a spherical wrist, the lowest value of the KDI ($KDI_{\text{min}} = 0.65$) was reached at $x = 280\,\text{mm}$ and $(\alpha = 0°, \beta = 90°, \gamma = 180°)$: this configuration is shown at the left of Figure 14 and shows that the robot is near the inner limit of its workspace. On the other hand, for the articulated robot with a non-spherical wrist, the lowest value of the KDI ($KDI_{\text{min}} = 0.51$) was reached at $x = 280\,\text{mm}$ and

($\alpha = 0°, \beta = 120°, \gamma = 180°$): this configuration is shown at the right of Figure 14 and is close to the elbow singularity.

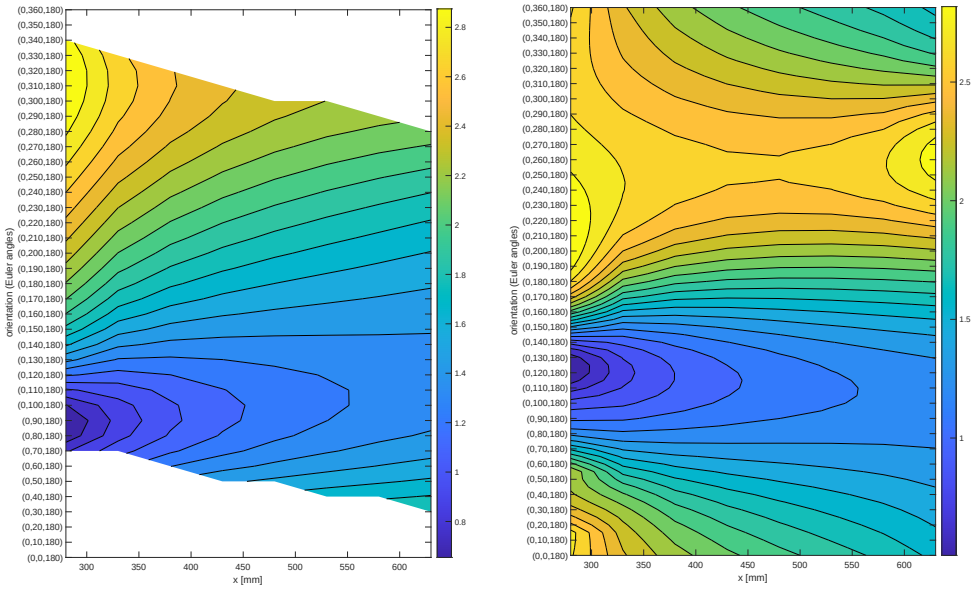

Figure 13. KDI investigation in terms of angular velocity ω_y with maximum joint speed set as 100 °/s for each joint for the articulated robot with a spherical wrist (**left**) and for the articulated robot with a non-spherical wrist and three consecutive joint axes (**right**).

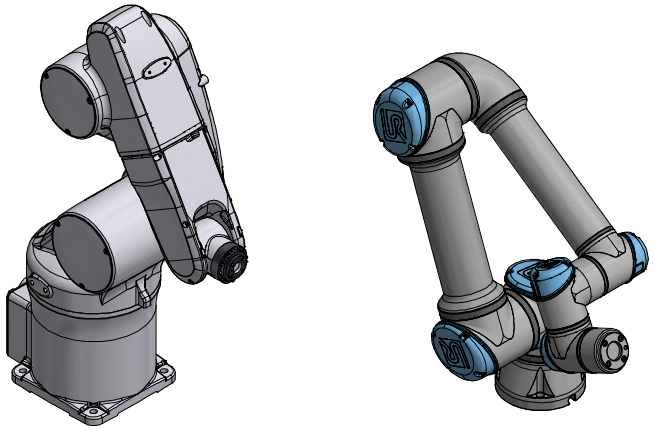

Figure 14. Configurations in which the two 6R architectures assume their lowest value of the KDI index in terms of angular velocity ω_y: (**left**) articulated robot with a spherical wrist, (**right**) articulated robot with a non-spherical wrist.

6. Conclusions

This paper has provided a kinematic comparison between two different 6R articulated robot architectures, the one with a spherical wrist and the one with a non-spherical wrist and three consecutive parallel axes, in terms of linear and angular velocity.

This work has highlighted that the difference in the structure of the wrist determines in fact a difference in the robot performance. In particular, for the articulated robot with a spherical wrist, the linear velocity in an horizontal plane is strongly correlated to the maximum speed of the third joint, whereas for the articulated robot with a non-spherical wrist, the linear velocity in the plane depends on the maximum speed of motors of both the third and fourth joints. Increasing respectively only the velocity of the third joint or both the third and fourth joint significantly increases the region of the workspace where a high velocity in the plane can be obtained. In addition, there is a strong relationship

between the linear velocity in the vertical plane of the articulated robot with a spherical wrist and the maximum speed of the second and fifth joint, while for the articulated robot with a non-spherical wrist, the linear velocity in the vertical plane is only correlated to the maximum speed of the second joint.

In terms of angular velocity, the wrist of the typical collaborative arm is more versatile and has a uniform behavior. On the other hand, the spherical wrist architecture can reach higher performance around a certain orientation. Moreover, a significant difference between the two wrists is that the structure of the spherical wrist imposes a limited range of θ_5, while the non-spherical wrist is more versatile and has usually a $\pm 360°$ range.

Author Contributions: The authors contributed equally to this work. All authors have read and agreed to the published version of the manuscript.

Funding: This research received no external funding.

Institutional Review Board Statement: Not applicable.

Informed Consent Statement: Not applicable.

Data Availability Statement: Not applicable.

Conflicts of Interest: The authors declare no conflict of interest.

Abbreviations

The following abbreviations are used in this manuscript:

MDPI	Multidisciplinary Digital Publishing Institute
DOAJ	Directory of open access journals
TLA	Three letter acronym
LD	Linear dichroism

References

1. Pieper, D. *The Kinematics of Manipulators under Computer Control*; Computer Science Department, Stanford University: Stanford, CA, USA 1968.
2. Wang, X.; Zhang, D.; Zhao, C. The inverse kinematics of a 7R 6-degree-of-freedom robot with non-spherical wrist. *Adv. Mech. Eng.* **2017**, *9*, 1687814017714985. [CrossRef]
3. Li, J.; Yu, H.; Shen, N.; Zhong, Z.; Lu, Y.; Fan, J. A novel inverse kinematics method for 6-DOF robots with non-spherical wrist. *Mech. Mach. Theory* **2021**, *157*, 104180. [CrossRef]
4. Hawkins, K.P. Analytic Inverse Kinematics for the Universal Robots UR-5/UR-10 Arms. 2013. Available online: https://smartech.gatech.edu/handle/1853/50782 (accessed on 29 December 2022).
5. Villalobos, J.; Sanchez, I.Y.; Martell, F. Statistical comparison of Denavit-Hartenberg based inverse kinematic solutions of the UR5 robotic manipulator. In Proceedings of the 2021 International Conference on Electrical, Computer, Communications and Mechatronics Engineering (ICECCME), Mauritius, Mauritius, 7–8 October 2021.
6. Kebria, P.M.; Al-wais, S.; Abdi, H.; Nahavandi, S. Kinematic and dynamic modelling of UR5 manipulator. In Proceedings of the 2016 IEEE International Conference on Systems, Man, and Cybernetics (SMC), Budapest, Hungary, 9–12 October 2016; pp. 004229–004234.
7. Villalobos, J.; Sanchez, I.Y.; Martell, F. *Alternative Inverse Kinematic Solution of the UR5 Robotic Arm*; Lecture Notes in Networks and Systems; Springer: Berlin/Heidelberg, Germany, 2022; Volume 347, pp. 200–207.
8. FarzanehKaloorazi, M.H.; Bonev, I.A. Singularities of the typical collaborative robot arm. In Proceedings of the ASME Design Engineering Technical Conference, Quebec City, QC, Canada, 26–29 August 2018; Volume 5B-2018.
9. Weyrer, M.; Brandstötter, M.; Husty, M. Singularity Avoidance Control of a Non-Holonomic Mobile Manipulator for Intuitive Hand Guidance. *Robotics* **2019**, *8*, 14. [CrossRef]
10. Villalobos, J.; Sanchez, I.Y.; Martell, F. Singularity Analysis and Complete Methods to Compute the Inverse Kinematics for a 6-DOF UR/TM-Type Robot. *Robotics* **2022**, *11*, 137. [CrossRef]
11. Wu, X.; Yan, R.; Xiang, Z.; Zheng, F.; Tan, R. Performance Analysis and Comparison of Three Planar Parallel Manipulators. In *Mechanisms and Machine Science*; Springer: Berlin/Heidelberg, Germany, 2020; Volume 79, pp. 270–279.
12. Baena, A.H.; Valdez, S.I.; de Jesús Trujillo Romero, F.; Montes, M.M. Comparison of Parallel Versions of SA and GA for Optimizing the Performance of a Robotic Manipulator. In *Mechanisms and Machine Science*; Springer: Berlin/Heidelberg, Germany, 2020; Volume 86, pp. 290–303.
13. Yoshikawa, T. Dynamic manipulability of robot manipulators. In Proceedings of the 1985 IEEE International Conference on Robotics and Automation, St. Louis, MO, USA, 25–28 March 1985; Volume 2, pp. 1033–1038.

14. Salisbury, J.K.; Craig, J.J. Articulated Hands: Force Control and Kinematic Issues. *Int. J. Robot. Res.* **1982**, *1*, 4–17. [CrossRef]
15. Angeles, J.; López-Cajún, C.S. Kinematic Isotropy and the Conditioning Index of Serial Robotic Manipulators. *Int. J. Robot. Res.* **1992**, *11*, 560–571. [CrossRef]
16. Gosselin, C.; Angeles, J. A Global Performance Index for the Kinematic Optimization of Robotic Manipulators. *J. Mech. Des.* **1991**, *113*, 220–226. [CrossRef]
17. Gao, F.; Liu, X.; Gruver, W.A. Performance evaluation of two-degree-of-freedom planar parallel robots. *Mech. Mach. Theory* **1998**, *33*, 661–668. [CrossRef]
18. Merlet, J.P. Jacobian, manipulability, condition number, and accuracy of parallel robots. *J. Mech. Des. Trans. ASME* **2006**, *128*, 199–206. [CrossRef]
19. Gosselin, C.M. The optimum design of robotic manipulators using dexterity indices. *Robot. Auton. Syst.* **1992**, *9*, 213–226. [CrossRef]
20. Kim, S.; Ryu, J. New dimensionally homogeneous Jacobian matrix formulation by three end-effector points for optimal design of parallel manipulators. *IEEE Trans. Robot. Autom.* **2003**, *19*, 731–737.
21. Kim, S..; Ryu, J. Force transmission analyses with dimensionally homogeneous jacobian matrices for parallel manipulators. *KSME Int. J.* **2004**, *18*, 780–788. [CrossRef]
22. Mansouri, I.; Ouali, M. A new homogeneous manipulability measure of robot manipulators, based on power concept. *Mechatronics* **2009**, *19*, 927–944. [CrossRef]
23. Mansouri, I.; Ouali, M. The power manipulability A new homogeneous performance index of robot manipulators. *Robot.-Comput.-Integr. Manuf.* **2011**, *27*, 434–449. [CrossRef]
24. Cardou, P.; Bouchard, S.; Gosselin, C. Kinematic-sensitivity indices for dimensionally nonhomogeneous jacobian matrices. *IEEE Trans. Robot.* **2010**, *26*, 166–173. [CrossRef]
25. Wang, J.; Liu, X.; Wu, C. Optimal design of a new spatial 3-DOF parallel robot with respect to a frame-free index. *Sci. China Ser. E Technol. Sci.* **2009**, *52*, 986–999. [CrossRef]
26. Wang, J.; Wu, C.; Liu, X. Performance evaluation of parallel manipulators: Motion/force transmissibility and its index. *Mech. Mach. Theory* **2010**, *45*, 1462–1476. [CrossRef]
27. Zhang, D.; Cursi, F.; Yang, G. Wsrender: A workspace analysis and visualization toolbox for robotic manipulator design and verification. *IEEE Robot. Autom. Lett.* **2019**, *4*, 3836–3843. [CrossRef]
28. Cursi, F.; Bai, W.; Yeatman, E.M.; Kormushev, P. GlobDesOpt: A Global Optimization Framework for Optimal Robot Manipulator Design. *IEEE Access* **2022**, *10*, 5012–5023. [CrossRef]
29. Boschetti, G. A novel kinematic directional index for industrial serial manipulators. *Appl. Sci.* **2020**, *10*, 5953. [CrossRef]